Robotica (2019) volume 37, pp. 1202–1213. © Cambridge University Press 2018
doi:10.1017/S0263574718000681

Multi-robot system optimization based on redundant serial spherical mechanism for robotic minimally invasive surgery

C. A. Nelson†, M. A. Laribi‡* and S. Zeghloul‡

†*Department of Mechanical and Materials Engineering, University of Nebraska-Lincoln, Lincoln, NE 68588-0526, USA*
‡*Department of GMSC, Pprime Institute, CNRS - University of Poitiers - ENSMA - UPR 3346, 86962 Futuroscope Chasseneuil Cedex, France*
Emails: cnelson5@unl.edu, said.zeghloul@univ-poitiers.fr

(Accepted July 12, 2018)

SUMMARY
Serial spherical linkages have been used in the design of a number of robots for minimally invasive surgery, in order to mechanically constrain the surgical instrument with respect to the incision. However, the typical serial spherical mechanism suffers from conflicting design objectives, resulting in an unsuitable compromise between avoiding collision with the patient and producing good kinematic and workspace characteristics. In this paper, we propose a multi-robot system composed of two redundant serial spherical linkages to achieve this purpose. A multi-objective optimization for achieving the aforementioned design goals is presented first for a single redundant robot and then for a multi-robot system. The problem of mounting multiple robots on the operating table as well as the way cooperative actions can be performed is addressed. The sensitivity of each optimal solution (single-robot and multi-robot) to uncertainties in the design parameters is investigated.

KEYWORDS: Multi-robot system, Serial spherical mechanism, Redundant linkage, Surgical robot, Minimally invasive surgery

1. Introduction

In minimally invasive surgery, the instruments are inserted through small incisions, which thereafter serve as kinematic constraints allowing four degrees of freedom (DOF) per instrument (three rotations centered at the incision point, often referred to as the remote center of motion,[3] and one translation through the incision).[18] Various spherical mechanisms have been proposed in the surgical robotics literature for mechanically constraining the instruments to avoid motions that would cause trauma to the tissue at the incision location.[1,4,5,6,11,14,15] Among these are serial spherical linkages, either actuated at each joint[2,16] or powered by actuators on a fixed base with motion transmitted through gearing,[17,18,19,20] cables,[7] or other means.

Parallel robots offer potential advantages compared with serial robots, including higher overall stiffness, higher precision, low inertia, and higher operating speeds and accelerations.[13,14] However, these advantages are offset by reduced workspace, difficult mechanical design, and more complex kinematics and control algorithms. The serial structure presents a natural choice due to the interference problem that results from closed loop structures.

The typical serial spherical mechanism has three intersecting rotation axes fixed in two links, providing the three rotational DOF mentioned previously. The angles of the two links must be chosen carefully in order to provide adequate workspace (usually considered as a cone whose apex half-angle is at least 30°[12]) without interference (collision) between the robot and the patient. However, these two primary design objectives are in opposition, as the larger links required to increase workspace also increase the impingement of the robot in the space occupied by the patient.

* Corresponding author. E-mail: med.amine.laribi@univ-poitiers.fr

https://doi.org/10.1017/S0263574718000681 Published online by Cambridge University Press

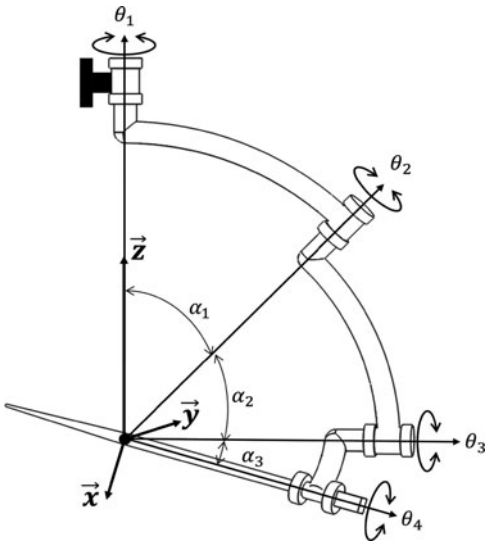


Fig. 1. Redundant serial spherical arm.

In this paper, we propose solving this problem by introducing an additional (redundant) link. We present a multi-objective optimization considering the workspace requirements, the kinematic performance, and the collision constraint. We also address the problem of multi-robot installation on an operating table.

2. Robot Design and Optimization Process

The proposed robot architecture is a classic serial spherical linkage (two links and three joints with intersecting axes) with a redundant link (and joint) added, as shown in Fig. 1. Singularities (well known for this type of robot) are avoided by restricting the motion of each joint to avoid alignment of adjacent links. We similarly avoid internal collisions within the robot itself. Thus, the robot remains in a single operating mode throughout its used workspace. The problem consists of finding the optimal link parameters, expressed as angles α_i, which satisfy the objectives and constraints mentioned previously.

The task-based synthesis and optimization of medical robots is a rich topic area in the literature.[3,8] Building from classical performance indices in robotics, specialized indices have been proposed to account for workspace requirements in this type of robot.[9,17] However, it is less common to see optimization approaches in medical robotics which account for the avoidance of collisions between the robot and the patient.

We adopt a multi-objective optimization approach considering workspace, kinematic performance, and robot compactness as criteria. For the workspace criterion, we recognize that the actual workspace will not be exactly equal to the conical section of a spherical surface described previously, so we base the optimization on a conservative measure of such an idealized workspace inscribed within the actual workspace. The actual workspace is directly calculated by forward kinematics, discretizing the joint space (in 5° increments) within the limited range of motion previously mentioned. Collision avoidance is directly accounted for within the optimization subroutine by throwing out any workspace points at which any part of the robot penetrates a planar boundary passing through the surgical incision and orthogonal to the neutral axis of the surgical trocar. Such cases are shown in Fig. 2. For the kinematic performance criterion, we use the improved indices proposed by Olds,[10] which give worst-case measures of position error (max) and velocity (min) in the two-dimensional workspace. Compactness is measured as the sum of the link angles α_i (this represents the total "angular space" occupied by the robot in its fully extended position).

As inputs, we use the three joint angles ($\theta_{1,2,3}$), and as outputs the pan (left-to-right) and tilt (down-to-up) angles intuitive to surgeons in the context of laparoscopic camera orientation. The joint angle θ_4 is not used as an input since it is for instrument self-rotation and does not affect tool position. Based

https://doi.org/10.1017/S0263574718000681 Published online by Cambridge University Press

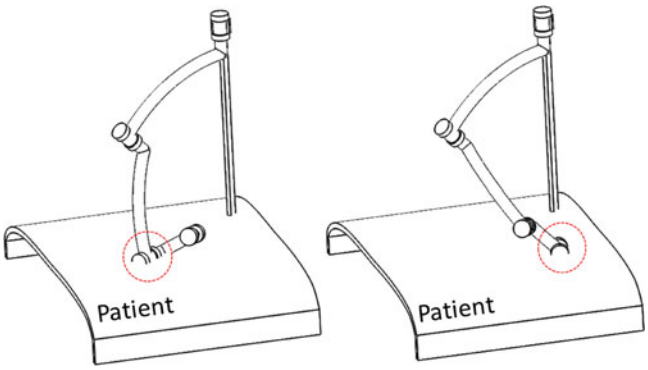


Fig. 2. Robot/patient collision cases (circle indicates area of collision).

on a neutral position with all robot links aligned and extended in the positive tilt direction:

$$p = \alpha_1 \sin\theta_1 + \alpha_2 \sin(\theta_1 + \theta_2) + \alpha_3 \sin(\theta_1 + \theta_2 + \theta_3) \tag{1}$$

$$t = \alpha_1 \cos\theta_1 + \alpha_2 \cos(\theta_1 + \theta_2) + \alpha_3 \cos(\theta_1 + \theta_2 + \theta_3) \tag{2}$$

where p is the pan angle and t is the tilt angle, and the Jacobian is

$$\mathbf{J} = \begin{bmatrix} J_{11} & J_{12} & J_{13} \\ J_{21} & J_{22} & J_{23} \end{bmatrix} \tag{3}$$

$$\begin{aligned}
J_{11} &= \alpha_1 \cos\theta_1 + \alpha_2 \cos(\theta_1 + \theta_2) + \alpha_3 \cos(\theta_1 + \theta_2 + \theta_3) \\
J_{12} &= \alpha_2 \cos(\theta_1 + \theta_2) + \alpha_3 \cos(\theta_1 + \theta_2 + \theta_3) \\
J_{13} &= \alpha_3 \cos(\theta_1 + \theta_2 + \theta_3) \\
J_{21} &= -\alpha_1 \sin\theta_1 - \alpha_2 \sin(\theta_1 + \theta_2) - \alpha_3 \sin(\theta_1 + \theta_2 + \theta_3) \\
J_{22} &= -\alpha_2 \sin(\theta_1 + \theta_2) - \alpha_3 \sin(\theta_1 + \theta_2 + \theta_3) \\
J_{23} &= -\alpha_3 \sin(\theta_1 + \theta_2 + \theta_3)
\end{aligned}$$

Because the robot is redundant, the Jacobian matrix is not square. Therefore, we adapt the indices[10] to include the pseudoinverse:

$$\mu_{\min} = \frac{1}{\max \mathbf{J}^*_{i\,2}} \tag{4}$$

$$\mu_{\max} = \max \frac{\mathbf{J}\dot{\theta}_2}{\dot{\theta}_\infty} \tag{5}$$

with the pseudoinverse of the Jacobian expressed as

$$\mathbf{J}^* = \mathbf{J}^{\mathrm{T}}\left(\mathbf{J}\mathbf{J}^{\mathrm{T}}\right)^{-1} \tag{6}$$

and $\mathbf{J}^*_i$ indicating the ith row of $\mathbf{J}^*$. Here, $\mu_{\min}$ represents the worst-case velocity, and $\mu_{\max}$ represents the worst-case position error. As suggested in ref. [10], we allow the velocity vector to take on its various possible extreme values in the calculation of $\mu_{\max}$:

$$\dot{\boldsymbol{\theta}} = \begin{Bmatrix} 1 \\ 1 \\ 1 \end{Bmatrix}, \begin{Bmatrix} 1 \\ -1 \\ 1 \end{Bmatrix}, \begin{Bmatrix} 1 \\ 1 \\ -1 \end{Bmatrix}, \begin{Bmatrix} 1 \\ -1 \\ -1 \end{Bmatrix} \tag{7}$$

https://doi.org/10.1017/S0263574718000681 Published online by Cambridge University Press

Table I. Parameter values used in optimization.

Parameter	Lower bound (°)	Upper bound (°)
$\alpha_{1,2,3}$	9	120
θ_1	−85	85
θ_2	5	175
θ_3	−175	−5

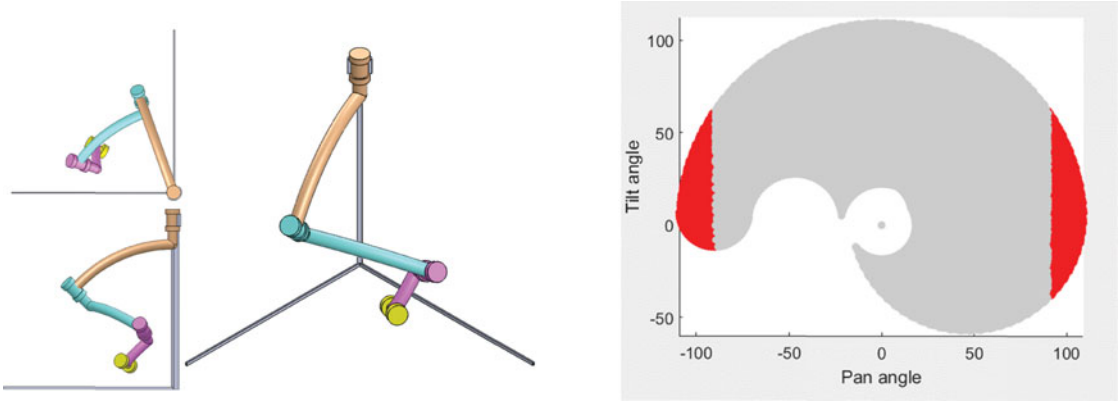


Fig. 3. The obtained redundant serial spherical mechanism: (left) computer rendering; (right) pan-tilt workspace—red area is excluded based on collision.

The kinematic performance is expressed as the worst of these two metrics ($\mu_{\min}$ and $\mu_{\max}$) at each point in the workspace and averaged across the entire feasible workspace (as sampled in the joint space).

The *fgoalattain*() function in MATLAB was used to carry out the optimization. This function is an implementation of the sequential quadratic programming method and allows multiple objectives to be weighted within a single objective function. In contrast to the Pareto approach, in which no criterion is allowed to get worse from one iteration to the next, the *fgoalattain*() function provides better convergence by allowing the search direction to experience "tradeoffs" between the individual criteria in order to optimize the global criterion.

The redundant serial arm was optimized using allowable ranges of the link parameters $\boldsymbol{\alpha}$ and joint variables $\boldsymbol{\theta}$ as indicated in Table I, and weights of 0 on workspace and collision avoidance, 0.3 on kinematic performance, and 0.5 on compactness (where 0 indicates a hard constraint and 1 represents an unenforced objective). These weights were chosen to enforce the need for safety and adequate workspace without completely neglecting the other desirable characteristics.

3. Optimization Results

The serial arm parameters obtained through optimization were $S : \{\alpha_1 = 46.7^\circ, \alpha_2 = 44^\circ, \alpha_3 = 18.9^\circ\}$. The resulting robot is shown in Fig. 3. The workspace and collision avoidance criteria are fully satisfied, and the kinematic performance of the robot can be seen in Fig. 4. As allowed by the *fgoalattain*() function, neither the performance nor the compactness criteria were fully satisfied; this is to be expected, as the robot is not expected to be perfectly small nor fully isotropic throughout the workspace.

The obtained result indicates that the algorithm performs in a stable manner and provides consistent results. Next, the variability of the optimized redundant serial spherical linkage performance generated by the design paramters will be estimated. Thus, the case of optimal solution S, given at the beginning of this section, will be studied.

https://doi.org/10.1017/S0263574718000681 Published online by Cambridge University Press

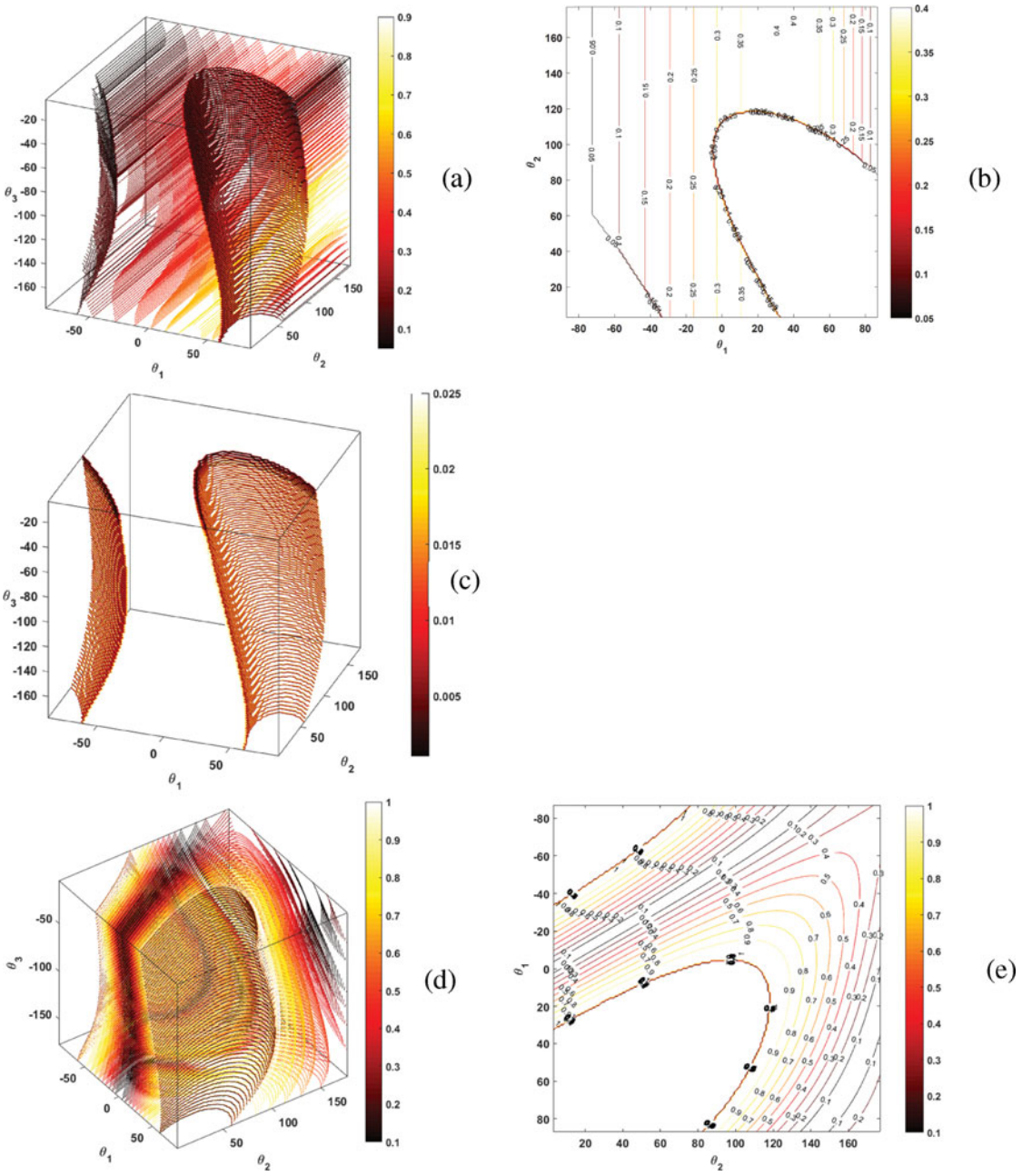


Fig. 4. Performance of optimized manipulator: (a) the distribution of μ in joint space; (b) the distribution of μ at $\theta_3 = -5^\circ$; (c) the distribution of $\mu_{\min}$ in joint space; (d) the distribution of the compactness criteria in joint space; (e) the distribution of the compactness criteria at $\theta_3 = -5^\circ$.

4. Multi-Robot Optimization

A practical implementation of this type of robot system may typically include multiple instances of the robot, each manipulating a different instrument. We now address the problem of multi-robot optimization, extending the problem presented in Section 2 by adding design parameters, constraints, and objectives. The problem consists of determining how to mount multiple robots on the operating table such that the robots avoid interfering with each other and yet possess a shared workspace inside the patient so that cooperative actions can be performed.

The multi-robot problem is expressed as shown in Fig. 5. To evaluate the conservative case most likely to produce robot–robot collision, the robots are placed opposite each other with the surgical trocars separated by a distance d. The θ_1 axis is mounted at an angle γ from the horizontal, shifting

https://doi.org/10.1017/S0263574718000681 Published online by Cambridge University Press

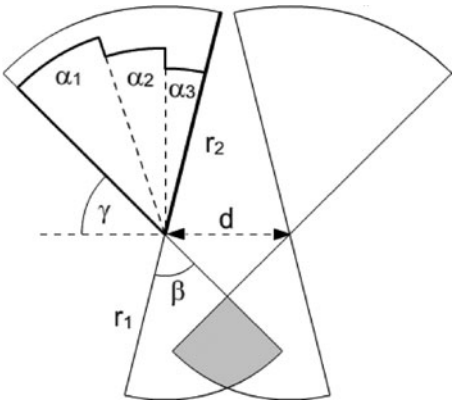


Fig. 5. Dual-robot layout and nomenclature.

the collision condition in the pan direction, with each robot mounted symmetrically. The laparoscope or other instrument carried by the robot is assumed to have a maximum penetration depth r_1 into the patient, and a maximum protruding distance r_2 outside the patient.

For given values of d, r_1, and r_2, the dual-robot system can be optimized with three slight modifications to the methods presented in Section 2. First, the parameter γ is added to the design vector. Second, a constraint for avoiding robot–robot collision is added. Based on Fig. 5 and a fully extended position of the robot, this consists of preventing the instruments' workspaces from overlapping, which can be formulated as an inequality constraint in the function call to *fgoalattain*():

$$\alpha_1 + \alpha_2 + \alpha_3 + \gamma \leq \pi - \cos^{-1}\left(\frac{d}{2r_2}\right) \tag{8}$$

Third and finally, a new objective is added to maximize the overlapping percentage of the workspace of each robot inside the patient. The total possible workspace is approximated (using the neutral plane representing a slice of the workspace volume) as the area of a section of a circle of radius r_1 with swept angle β:

$$A_0 = \frac{\beta}{2\pi}\pi r_1^2 = \frac{\beta r_1^2}{2} \tag{9}$$

where

$$\beta = \beta_{\max} - \beta_{\min} = (\alpha_1 + \alpha_2 + \alpha_3 + \gamma) - (\alpha_1 - \alpha_2 + \alpha_3 + \gamma) = 2\alpha_2 \tag{10}$$

This formulation of β is based on a fully extended arm ($\beta_{\max}$) and a fully folded (zigzag) arm ($\beta_{\min}$). To approximate the overlapping area, multiple cases must be considered. As shown in Fig. 6, the workspace boundaries are given by two pairs of lines and two circular arcs of radius r_1. The lines (A, B, C, D) may intersect either inside or outside the "useful" range $[0\ r_1]$. The common overalapping area A_c is zero if lines B and C intersect at a point outside the useful range.

Case 1: If all four intersections (AD, AC, BC, BD) are in the useful range, the overlapping area is a diamond. Due to the symmetry of the problem formulation, the area of the diamond is easily calculated as

$$A_c = \frac{\mathrm{d}x \cdot \mathrm{d}y}{2} \tag{11}$$

where dx and dy are the height and width of the diamond as given by the coordinates of the intersection points.

Case 2: If the intersection AD lies outside the useful range but the other three intersections lie inside the range, the intersection point of the two circular arcs can be used in place of intersection point AD to approximate the overlapping area as a diamond.

https://doi.org/10.1017/S0263574718000681 Published online by Cambridge University Press

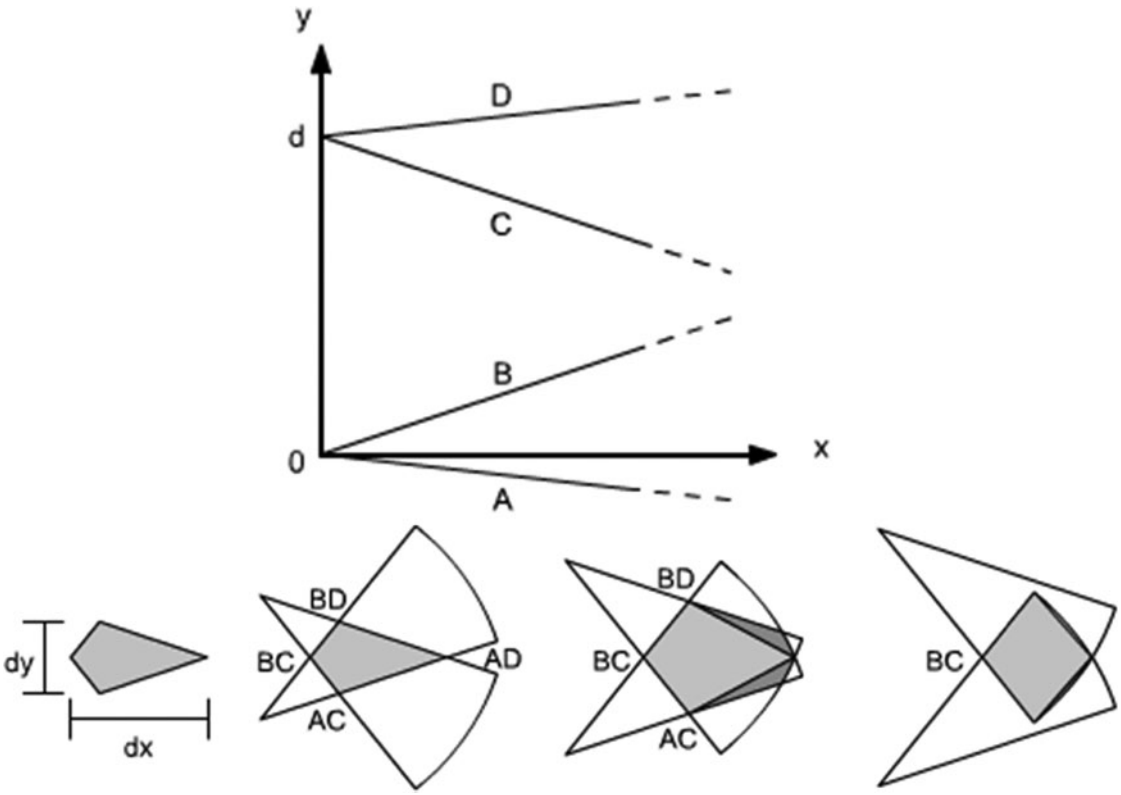


Fig. 6. Overlapping internal workspaces.

Case 3: If only intersection *BC* is in the useful range, the circular arc intersection as well as the endpoints of lines *B* and *C* are used to approximate the diamond.

To calculate the four intersection points, the lines are expressed as linear equations which are solved simultaneously. The slopes are

$$m_A = -m_D = \tan\left(\frac{\pi}{2} - \beta_{\max}\right) \tag{12}$$

$$m_B = -m_C = \tan\left(\frac{\pi}{2} - \beta_{\min}\right) \tag{13}$$

and the *y*-intercepts are known to be 0 for lines *A* and *B* and *d* for lines *C* and *D*. Due to symmetry, the *y*-locations of intersections *BC* and *AD* (as well as the arc intersections) are known to take a value of $d/2$ (see Fig. 6). With this information, the intersection coordinates are solved, giving

$$x_{BC} = \frac{d}{2m_B} \tag{14}$$

$$x_{AD} = \frac{d}{2m_A} \tag{15}$$

$$x_{AC} = x_{BD} = \frac{d}{(m_A - m_C)} \tag{16}$$

$$y_{AC} = m_A x_{AC} \tag{17}$$

$$y_{BD} = m_B x_{BD} \tag{18}$$

The endpoint of line segment B (used in Case 3) has

$$y_B = r_1 \cos\beta_{\min} \tag{19}$$

https://doi.org/10.1017/S0263574718000681 Published online by Cambridge University Press

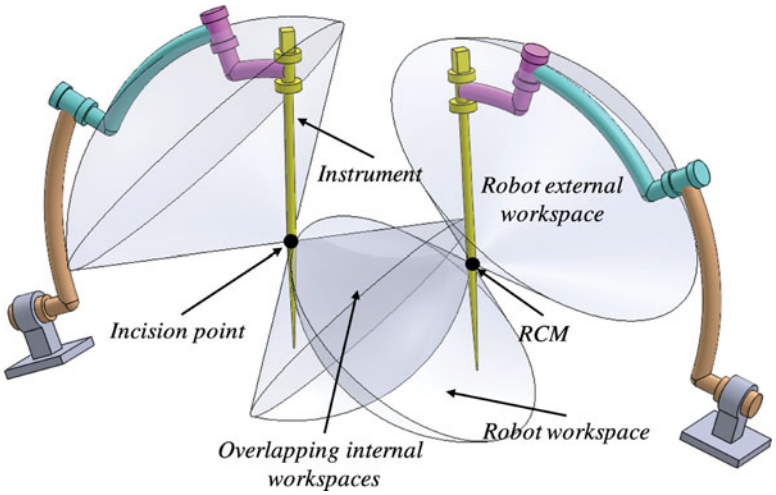


Fig. 7. Optimized two-robot system.

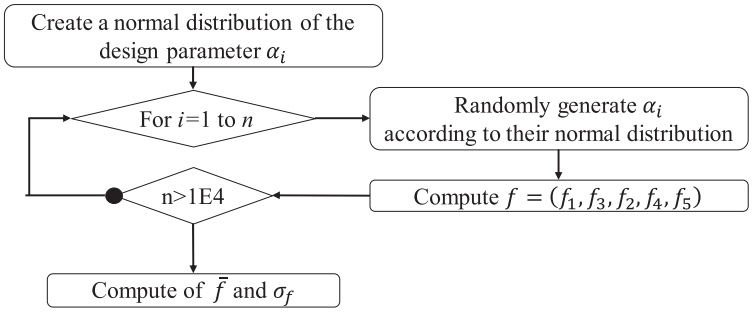


Fig. 8. Monte Carlo simulation flowchart.

and symmetry about the line $y = d/2$ gives the endpoint y_C and the corresponding diamond width. With these equations for Cases 1–3 as illustrated in Fig. 6, the overlapping area can be calculated using Eq. (11) and the objective for maximization in the optimization function is simply the ratio of A_c to A_0.

With this addition to the optimization algorithm as presented in Section 2, the optimization was repeated with γ constrained to the range $[-\pi/4\ \pi/2]$ and given an initial value of 0. The weighting factor for maximizing internal overlapping area was set at 0.2, with the other weights and constraints as previously presented in Section 2. Based on typical laparoscopic instrumentation and procedures, the trocar separation distance d was given a value of 15 cm, the instrument protrusion r_2 was given a value of 25 cm, and the maximum insertion depth r_1 was given a value of 15 cm. The serial arm parameters obtained through optimization were $S2 : \{\alpha_1 = 48.0^\circ,\ \alpha_2 = 42.8^\circ,\ \alpha_3 = 20.6^\circ\}$, with $\gamma = -40.2^\circ$. The resulting multi-robot system is shown in Fig. 7. The workspace and collision avoidance criteria are fully satisfied, and the overlapping workspace is at 62%. Note that the negative value of γ permits the robot to retain its large workspace (this solution is only slightly different from the single-robot solution presented at the beginning of Section 3) while avoiding robot–robot collisions.

5. Robustness Assessment

Next, the variability of the optimized redundant serial spherical linkage performance generated by the design parameters will be estimated. Thus, the case of optimal solution $S2$ obtained through the multi-objective optimization process, at the end of the previous section, will be studied. Each uncertain design parameter is represented by a statistical distribution. For a normal distribution, this requires a mean value and a standard deviation. A Monte Carlo simulation[13] is performed for every design parameter where each evaluation consists of a specified number of runs as shown in Fig. 8.

https://doi.org/10.1017/S0263574718000681 Published online by Cambridge University Press

Table II. Sensitivity of the optimal solution.

Objective function	Mean value $\overline{f_i}$	Standard deviation σ_{f_i}	Sensitivity s_i
Workspace: f_1	−0.056	0.0228	−120.8%
Collision: f_2	−0.49	0.0044	2.65%
Kinematic performance: f_3	0.56	0.0026	1.36%
Compactness: f_4	0.42	0.0162	11%
Internal overlapping area: f_5	0.9	0.0190	6.5%

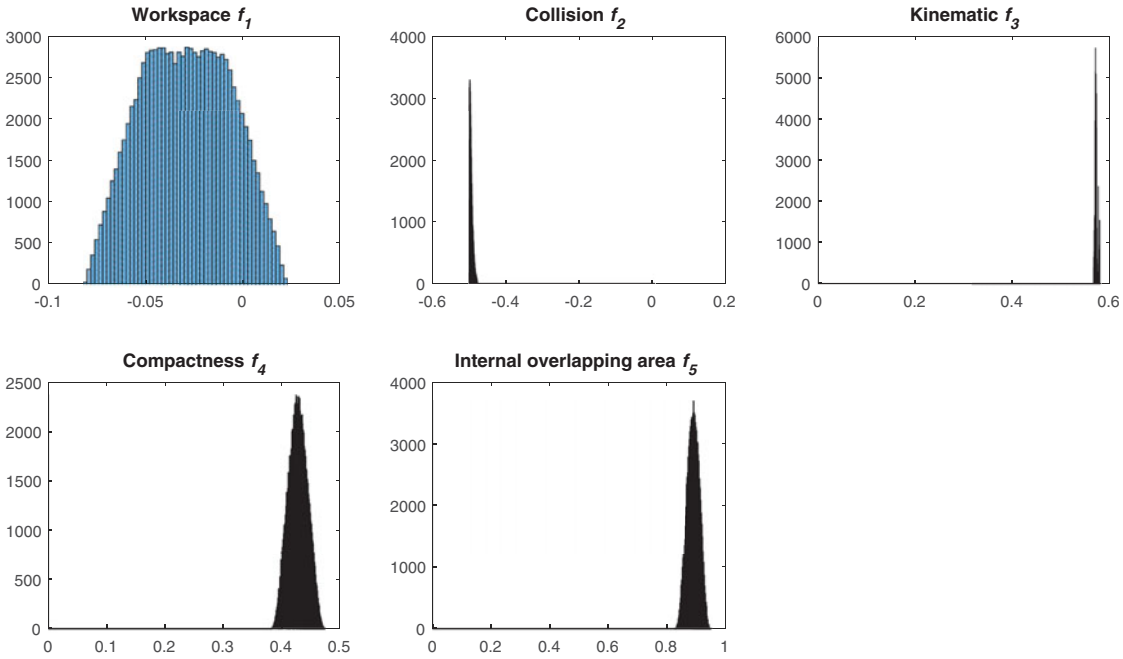


Fig. 9. Effect of the design parameters' uncertainty on the objective functions.

For each Monte Carlo simulation, all the deterministic design variables, α_i, are fixed at their nominal values and the uncertain design variables, $\tilde{\alpha}_i$, are selected randomly from their statistical distributions assumed to vary within ±5% of the specified nominal values. With the Monte Carlo simulation, we perform $n = 10^5$ simulations to determine the mean value $\bar{f} = \{\bar{f}_1, \bar{f}_2, \bar{f}_3, \bar{f}_4, \bar{f}_5\}$ as well as the respective standard deviations $\sigma_f = \{\sigma_{f_1}, \sigma_{f_2}, \sigma_{f_3}, \sigma_{f_4}, \sigma_{f_5}\}$. The evolution of each performance is presented in Fig. 9. The sensitivity study result of the optimal solution S is shown in Table II.

We observe through these data the high sensitivity of the multi-robot system only on the first criterion concerning the workspace. For the case of a system with two robots, the maximization of the internal overlapping area consolidates the robustness of the collision criterion. In the case of a system with a single robot, the second criterion, collision, presents a high sensitivity as concluded in our previous work.[21]

The variation around the optimal values of the design parameters leads to a large violation of the performance criterion in relation with the workspace. This first observation justifies the choice of the very strict condition, equal to zero, on the respective weight at the definition of the optimization problem.

In contrast, the other criteria, respectively, collision, kinematic performance, compactness, and internal overlapping area, are less sensitive to the disturbance of the design parameters. The calculated sensitivities are between 1.36% and 11% which are still far from the workspace sensitivity.

Consequently, by considering the uncertainties of the design parameters the workspace given by the optimal solution S is no longer guaranteed within ±5% variation of the specified nominal values. One concludes that the quality of the optimal solution is given by the level of violation of the performance criterion.

https://doi.org/10.1017/S0263574718000681 Published online by Cambridge University Press

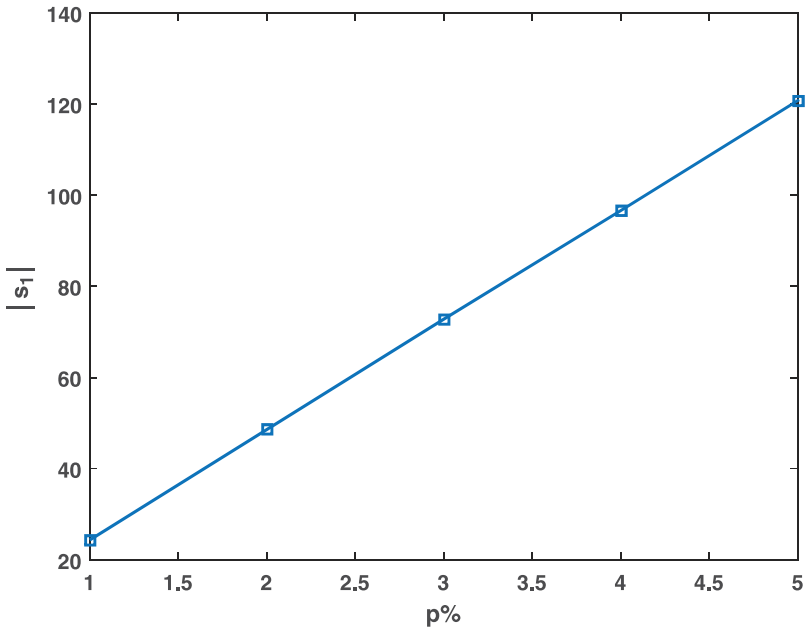


Fig. 10. Workpace sensitivity vs. distribution percentage.

The sensitivity level depends on the uncertain design variables, $\tilde{\alpha}_i$, selected randomly around nominal values. This selection is done inside an interval with statistical distributions assumed to vary within $\pm p\%$ of the specified nominal values. Figure 10 depicts the evolution of optimal solution quality linked to workspace objective function for different values of percentage variation. Linear evolution is observed. Percentage rise leads to an increase in sensitivity.

The impact of the uncertain design variables on the optimal solution and specifically on the workspace could be measured using the standard deviation. The angles sum $(\alpha_2 + \alpha_3)$ can be computed using the objective function definition f_1 and standard deviation value as follows:

$$(\alpha_2 + \alpha_3) = -\left((f_1 \pm \sigma) - 1\right) p_{\max} \tag{20}$$

Here, $p_{\max}$ represents the target angle for the *pan* direction considered equal to 60°.

After replacing the objective function and standard deviation values in Eq. (20), the angles sum moves inside the range 59.25° to 67.46° which leads to a maximum overlapping of 12.4% of $p_{\max}$. Figure 11 presents the variation of the angles sum and the corresponding overlapping for $\pm\sigma$, $\pm 2\sigma$, and $\pm 3\sigma$, repectively.

The user could define a distribution percentage to select the more robust solution depending on the task specifications. If the distribution percentage is selected such that the workpace sensitivity is reduced, than the optimal solutions obtained by the multi-objective optimization can be considered robust.

6. Conclusions

In this work, a redundant serial spherical linkage has been presented to cope with the problems of the classic serial spherical mechanism for medical robots. Four design objectives have been presented and adapted to the proposed redundant mechanism: workspace, kinematic performance, avoiding collision, and compactness. A multi-objective optimization problem is formulated in this aim and solved using the *fgoalattain*() function. The obtained optimal solution perfectly satisfies the workspace criterion as well as the collision avoidance requirement. However, neither the performance nor the compactness criteria were fully satisfied and this is due to the tradeoffs allowed by the optimization method. This type of result facilitates the designer's choice of a suitable solution by generating a specific solution without going through a Pareto front. Furthermore, a multi-robot scenario was optimized to maximize shared workspace within the patient while avoiding external collisions. A sensitivity study is

https://doi.org/10.1017/S0263574718000681 Published online by Cambridge University Press

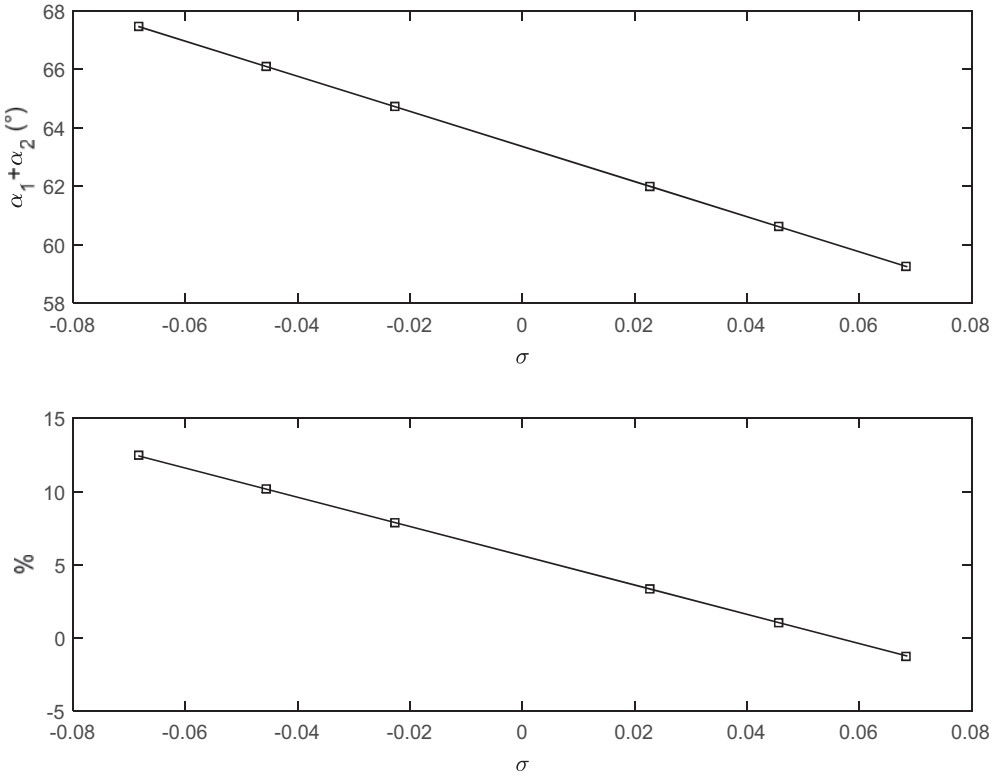


Fig. 11. Evolution of $(\alpha_2 + \alpha_3)$ and its overlapping vs. standard deviation.

performed based on the Monte Carlo method which shows that the deterministic optimal solutions can be strongly affected by the uncertainties in the design parameters. A suitable distribution percentage choice leads to a reduced sensitivity and specifically the workspace sensitivity. In this case, the optimal solution obtained by the multi-objective optimization can be considered robust. The sensitivity level can be addressed at the beginng of the user requirements definition. This level could be handled by the multi-objective optimization to directly obtain, if feasable, a robust solution.

Acknowledgment

This work is sponsored by the French government research program Investissements d'avenir through the Robotex Equipment of Excellence (ANR-10-EQPX-44) and by a faculty development fellowship from the University of Nebraska-Lincoln.

References

1. P. Berkelman, E. Boidard, E. Cinquin and J. Troccaz, "LER: The Light Endoscope Robot," *Proceedings of IEEE/RSJ International Conference on Intelligent Robots and Systems IROS*, Las Vegas, NV, USA (2003) pp. 2835–2840.
2. F. Courreges, N. Smith-Guerin, G. Poisson, P. Vieyres, A. Gourdon, M. Szpieg and O. Merigeaux, "Real-Time Exhibition of a Simulated Space Tele-Echography Using an Ultra-Light Robot," *Proceedings of the International Symposium on Artificial Intelligence, Robotics and Automation in Space ISAIRAS*, Canada (2001).
3. B. Eldridge, K. Gruben, D. LaRose, J. Funda, S. Gomory, J. Karidis, G. McVicker, R. Taylor and J. Anderson, "A remote center of motion robotic arm for computer assisted surgery," *Robotica* **14**(1), 103–109 (1996).
4. T. Essomba, L. Nouaille, M. A. Laribi, C. A. Nelson, S. Zeghloul and G. Poisson, "Spherical wrist dimensional synthesis adapted for tool-guidance medical robots," *Mech. Ind.* **15**(3), 217–223 (2014).
5. H. Kang and J. T. Wen, "EndoBot: A Robotic Assistant in Minimally Invasive Surgeries," *Proceedings of the IEEE International Conference on Robotics and Automation*, Seoul, South Korea (2001) pp. 2031–2036.
6. M. A. Laribi, T. Rivière, M. Arsicault and S. Zeghloul, "A Design of Slave Surgical Robot Based on Motion Cpture," *Proceedings of the 2012 IEEE International Conference on Robotics and Biomimetics (ROBIO2012)*, Guangzhou, China (Dec. 11–14, 2012) pp. 600–605.

https://doi.org/10.1017/S0263574718000681 Published online by Cambridge University Press

7. C. A. Nelson and X. Zhang, "Equivalent Mechanisms Techniques for Redesign of a Spherical Surgical Tool Manipulator," *Proceedings of the International Design Engineering Technical Conferences & Computers and Information ASME IDETC2010*, Montréal, Québec, Canada, (Aug. 15–18, 2010), ASME Paper No. DETC2010-28367 (2010).
8. L. Nouaille, M. A. Laribi, C. A. Nelson, T. Essomba, G. Poisson and S. Zeghloul, "Design process for robotic medical tool-guidance manipulators," *Proc. IMechE Part C: J. Mech. Eng. Sci.* **230**(2), 259–275 (2016).
9. L. Nouaille, G. Poisson, X. Zhang and C. A. Nelson, "Method of dimensional optimization of spherical robots for medical applications using specialized indices," *Adv. Robot.* **28**(3), 173–186 (2014).
10. K. Olds, "Global indices for kinematic and force transmission performance in parallel robots," *IEEE Trans. Robot.* **31**(2), 494–500 (2015).
11. H. Rininsland, "ARTEMIS. A telemanipulator for cardiac surgery," *Eur. J. Cardio-Thoracic Surg.* **16**(2), 106–111 (1999).
12. J. Rosen, J. D. Brown, L. Chang, M. Barreca, M. Sinanan and B. Hannaford, "The BlueDRAGON – a System for Measuring the Kinematics and the Dynamics of Minimally Invasive Surgical Tools In-Vivo," *Proceedings of the IEEE International Conference on Robotics and Automation*, Washington, DC (2002) pp. 1876–1881.
13. I. Ebert-Uphoff, C. M. Gosselin and T. Laliberté, "Static balancing of spatial parallel platform mechanisms – revisited," *J. Mech. Des. Trans. ASME* **122**(1), 43–51. doi:10.1115/1.533544 (2000).
14. D. Cafolla, G. Carbone and M. Ceccarelli, "Balancing of a 3-dofs Parallel Manipulator," **In**: *Dynamic Balancing of Mechanisms and Synthesizing of Parallel Robots*, (2016) pp. 173–191, DOI: 10.1007/978-3-319-17683-3_8.
15. M. Schinozuka, "Monte Carlo solution of structural dynamics," *Comput. Struct.* **2**, 855–874 (1972).
16. T. K. Tanev, A. Cammarata, D. Marano and R. Sinatra, "Elastostatic Model of a New Hybrid Minimally Invasive Surgery Robot," *Proceedings of the 14th IFToMM World Congress*, Taipei, Taiwan (Oct. 25–30 2015).
17. C. Vaida, B. Gherman, D. Pisla and N. Plitea, "A Spherical Robot Arm for Instruments Positioning in Minimally Invasive Medical Applications," *Proceedings of the 2nd IFToMM Asian Conference on Mechanism and Machine Science*, Tokyo, Japan (Nov. 7–10 2012).
18. N. Zemiti, T. Ortmaier, M. A. Vitrani and G. Morel, "A Force Controlled Laparoscopic Surgical Robot Without Distal Force Sensing," *Proceedings of the 9th International Symposium on Experimental Robotics ISER'04*, Singapore (2004).
19. X. Zhang and C. A. Nelson, "Multiple-criteria kinematic optimization for the design of spherical serial mechanisms using genetic algorithms," *J. Mech. Des.* **133**(1), 011005 (2011).
20. X. Zhang and C. A. Nelson, "Kinematic analysis and optimization of a novel robot for surgical tool manipulation," *J. Med. Devices* **2**(2), 021003 (2008).
21. C. A. Nelson, M. A. Laribi and S. Zeghloul, "Optimization of a Redundant Serial Spherical Mechanism for Robotic Minimally Invasive Surgery," *Proceedings of the 7th International Workshop on Computational Kinematics, Futuroscope-Poitiers*, France (May 2017), Mechanisms and Machine Science, Vol. 50, Springer, (2017) ISBN 978-3-319-60866-2.

https://doi.org/10.1017/S0263574718000681 Published online by Cambridge University Press